ELSEVIER

Cement & Concrete Composites 26 (2004) 389–404

Cement & Concrete Composites

www.elsevier.com/locate/cemconcomp

Cracking response and local stress characteristics of RC membrane elements reinforced with welded wire mesh

Masoud Soltani [a,*], Xuehui An [b], Koichi Maekawa [a]

[a] Department of Civil Engineering, The University of Tokyo, Hongo 7-3-1, Bunkyo-ku, Tokyo 113, Japan
[b] Department of Hydraulic Engineering, Tsinghua University, Beijing 100084, China

Received 16 April 2002; accepted 20 February 2003

Abstract

The purpose of this study is to investigate the structural behavior and cracking response of RC membrane elements reinforced with welded wire mesh subjected to general in-plane stresses. The response of RC elements is computed based on micro mechanisms of stress transfer in RC domain involving interaction of concrete and reinforcing bars, anchorage effect of longitudinal and transverse wires and stress transfer across cracks due to aggregate interlock. The effect of type and arrangement of longitudinal and transverse wires on the structural behavior such as ductility, crack width and also on the spatial post cracking constitutive models of RC elements is described.

Keywords: RC; Membrane element; Crack; Tension stiffening; Welded wire mesh

1. Introduction

For many years, the prefabricated welded wire mesh has been used in both precast and on-site concrete constructions, such as slabs, bridge decks, highways and walls, and as shear reinforcements in RC members. Considerable financial and time saving and also the facility in quality control, are some benefits for substituting the distributed longitudinal and transverse conventional reinforcing bar by prefabricated welded wire mesh.

Many research activities during the past have been undertaken to investigate cracking response and structural behavior of reinforced concrete members, reinforced with deformed bars or developing conceptual constitutive models for these structures. However, little effort has been done to analytically investigate the influence of welded wire mesh on the cracking response and the structural behavior.

Ayyub et al. [1] conducted pullout test on welded wire mesh with different types of anchorage details. They concluded that by using welded wire fabric, the pullout strength increased in the range of 16% to 771% due to the large contribution of transverse wires as the anchorage for longitudinal bars. Lee et al. [2] experimentally studied the crack spacing and width in RC members subjected to direct tension and flexural moment. They found that the crack spacing and width considerably decreased using welded wire fabric however this reduction strictly depended on arrangement and type of wires. Large bond strength and crack control characteristics of welded wire fabric have led researchers to investigate the effectiveness of welded wire fabrics as shear reinforcement in RC members [3].

Vecchio and Collins [4,5] in development of so-called "modified compression field theory", for analyzing RC elements subjected to in-plane stresses, experimentally investigated the cracking behavior of these elements. The famous experimental work of Vecchio and Collins, that is mainly on RC elements reinforced with welded wire mesh, was later used by many researchers for development or verification of constitutive models of RC elements reinforced with deformed bars [6–8]. But actually, the stress transfer system in RC panels reinforced with welded wire mesh is quite different from those reinforced with deformed bars. Due to this fact and based on experimental results on RC specimen

* Corresponding author. Fax: +81-3-5841-6010.
E-mail address: masouds@concrete.t.u-tokyo.ac.jp (M. Soltani).

0958-9465/$ - see front matter © 2003 Elsevier Ltd. All rights reserved.
doi:10.1016/S0958-9465(03)00035-0

reinforced with deformed bar, Okamura and Maekawa [9] empirically proposed two different tension stiffening models for welded wire mesh and deformed bars as shown in Fig. 1(a).

As a matter of fact, the experimental results on RC elements show very large scatter in tensile stress mobilized in cracked concrete (see Fig. 1(b)) that is not obvious in RC specimens subjected to direct tension [10,11]. Even though the simple expression of tension stiffening model is acceptable for middle or highly reinforced concrete elements (reinforced in two orthogonal directions), the tensile stress transfer ability of cracked concrete in RC element with low reinforcement ratio in one or both directions strictly affects the cracking response, failure mode and capacity of these elements. In addition, the welded wire fabric used in experimental work of Vecchio and Collins [4] was made from small sized plain bars set at small spacing (mainly 50 mm), however the spacing and type of wires have a considerable effect on cracking response and ductility of these elements.

The work described herein aims at development of a computational method for analysis of RC membrane elements reinforced with welded wire mesh based on the micro mechanism of stress transfer in RC domain.

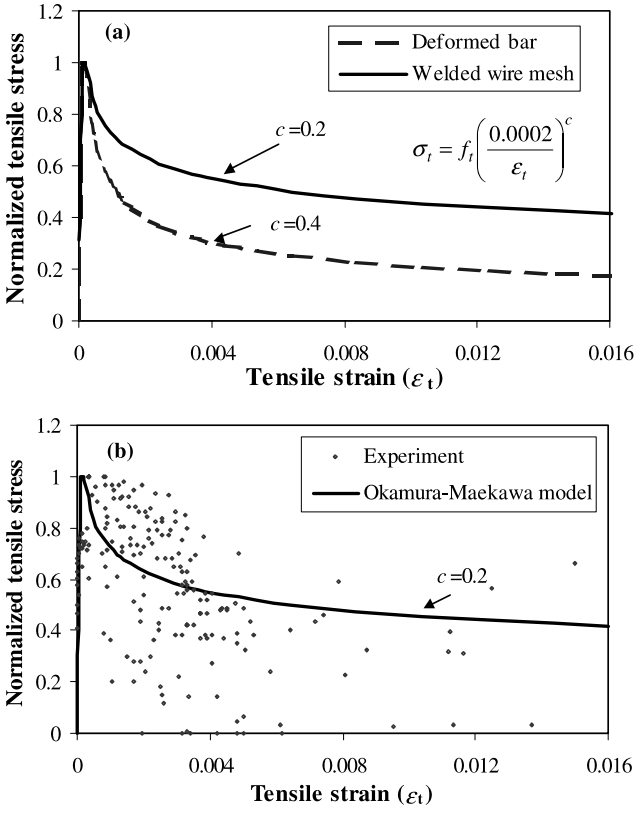

Fig. 1. Tension stiffening: (a) models for deformed bar and welded wire mesh; (b) comparison with available data in RC panels.

The proposed methodology is used: (1) to investigate the effect of type and arrangement of longitudinal and transverse wires on cracking response and structural behavior of these elements; (2) to investigate the spatially averaged post cracking constitutive models of RC membrane elements reinforced with welded wire mesh involving tension stiffening and average yield strength of reinforcing bars; (3) to compare the results with the case of RC elements reinforced with conventional deformed bars.

The systematic verification of the proposed method is carried out through comparison with some experimental results and subsequently is used for parametric investigation.

2. Local and average stress states in cracked RC elements

Fig. 2(a) shows the state of stresses of a reinforced concrete element subjected to general in-plane stresses in coordinate system x–y. The RC element is orthogonally reinforced with longitudinal and transverse bars placed in x and y directions, respectively. The principal direction of the applied stresses is defined by 1–2 coordinate system (Fig. 2(b)). The crack direction is initially considered normal to principal direction of tensile stress (at angle θ with respect to x direction). After cracking, the local stress and strain states in RC elements change (Fig. 2(c)). At a distinct cracked section, the local force normal to crack is carried by reinforcing bars (f_{crx} and f_{cry}) and bridging stress of cracked concrete (σ_{br}). The local force across crack is carried by aggregate interlock (τ_{agg}) and dowel action of reinforcing bars (τ_s). Due to interlocking of aggregates at crack plane, the compression stress, so called "dilatancy stress (σ_d)", is applied normal to the crack surface.

The local force of reinforcing bars at the crack plane is partly transferred to the concrete between adjacent cracks through bond stress and anchorage effect of longitudinal and transverse wires (in case of welded wire mesh), while the bridging stress and stresses due to aggregate interlock (crack dilatancy and shear stress) and dowel action at crack location are directly applied to the fracturing planes.

Consequently, the stresses of concrete and reinforcing bar in the RC domain between cracks are different from the stress state at the crack plane. For the smeared model of cracked RC elements in FEM, the internal stresses of concrete and reinforcing bars, developing between adjacent cracks are mathematically treated by spatial average stress–average strain relationship of concrete and reinforcing bars which should coincide well with the local characteristics of stresses at the crack plane as well as stress transfer ability of concrete between adjacent cracks.

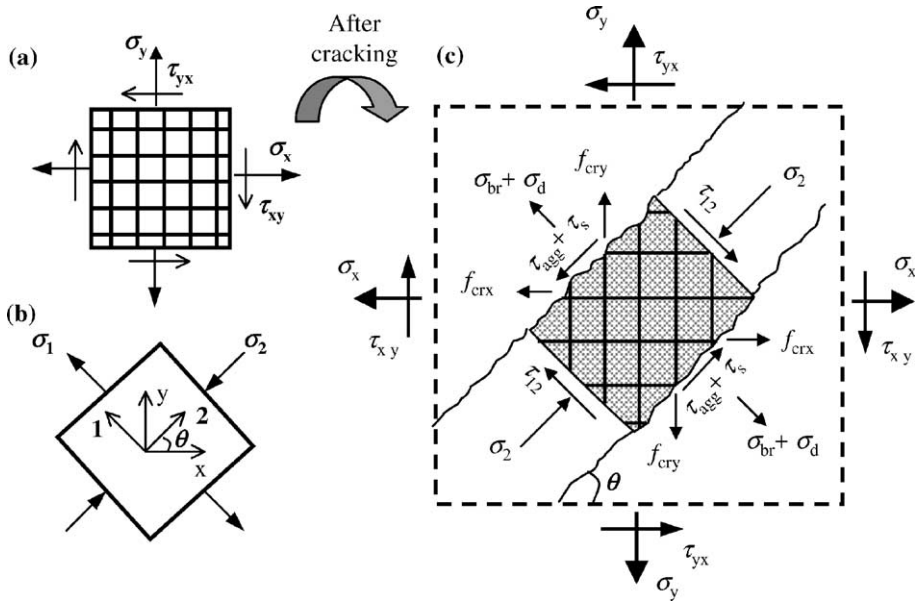

Fig. 2. RC element subjected to in-plane stresses: (a) applied stresses; (b) principal directions; (c) local stress state at cracked plane.

3. Micro-computational modeling of stress transfer along the reinforcing bars

In RC elements reinforced with welded wire mesh, the tensile stresses of reinforcing bars are transferred to the concrete through two main mechanisms: reinforcing bars-concrete bond and anchorage effect of reinforcements. Owing to these two mechanisms, after cracking, concrete continues to carry tensile stress between adjacent cracks and the stress–strain relationship of reinforcing bars, on average, is consequently different from bare bar behavior (Fig. 3). Steel at the crack location starts to yield before other points along its axis, and as a result, shows lower average yield stress compared to the bare bar. After yielding of reinforcement, some areas close to cracks come into the hardening zone, while the remaining areas are still in the elastic zone.

The transfer of stress from reinforcing bars to the concrete owing to the bond is due to the three components of adhesion, friction and mechanical interlock. The bond stress characteristic of plain bars depends mainly on adhesion and friction, while in the case of deformed bars the mechanical interlock of ribs governs the bond stress value. In RC elements reinforced with welded wire mesh both types of reinforcing bar may be used.

For deformed reinforcing bars in the present paper, the universal bond-slip-strain model proposed by Shima et al. [10] that is applicable for both elastic and post-yield range is used. The effect of elasticity, hardening strain and the stiffness in strain hardening zone, in other words the strain–stress characteristics of bare bar, is considered in this model. The local bond stress $\tau(\varepsilon, s_b)$ is expressed as

$$\tau(\varepsilon, s_b) = \tau_0(s_b) g(\varepsilon) \tag{1}$$

$$\tau_0(s_b) = f'_c k [\ln(1 + 5 s_b)]^C \tag{2}$$

$$g(\varepsilon) = \frac{1}{1 + 10^5 \varepsilon} \tag{3}$$

where, $\tau_0(s_b)$ is intrinsic bond stress when strain is zero, f'_c is compressive strength of concrete, C is constant equal to 3, k is constant equal to 0.73, s_b is non-dimensional slip equal to $1000 S_b/D_b$, S_b is absolute value of slip (axial deformation of steel bar) and D_b and ε are diameter and steel strain respectively.

In the case of plain bar the CEB-FIP model code [12] is adopted in this work. The local bond stress between concrete and reinforcing bars is defined as a function of relative displacement as

$$\tau(S_b) = \tau_u \left(\frac{S_b}{S_{b1}} \right)^{0.5}, \quad 0 \leqslant S_b < S_{b1}$$

$$\tau(S_b) = \tau_u, \quad S_b \geqslant S_{b1} \tag{4}$$

where, S_b is relative displacement between concrete and reinforcing bars (difference between axial deformation of steel and concrete), S_{b1} is maximum slip before bond plasticity and is considered 0.01 mm for cold drawn wires and 0.1 mm for hot rolled bars, τ_u is bond capacity, that depends on many factors especially the confinement effect due to lateral pressure and bond conditions. The influence of confinement on bond capacity of plain bars has been studied [13,14] and it has been shown that the bond capacity increases by increasing the confinement, however a confinement of more than $0.25 f'_c$ has less effectiveness on increasing bond capacity. The CEB-FIP model code, considers the

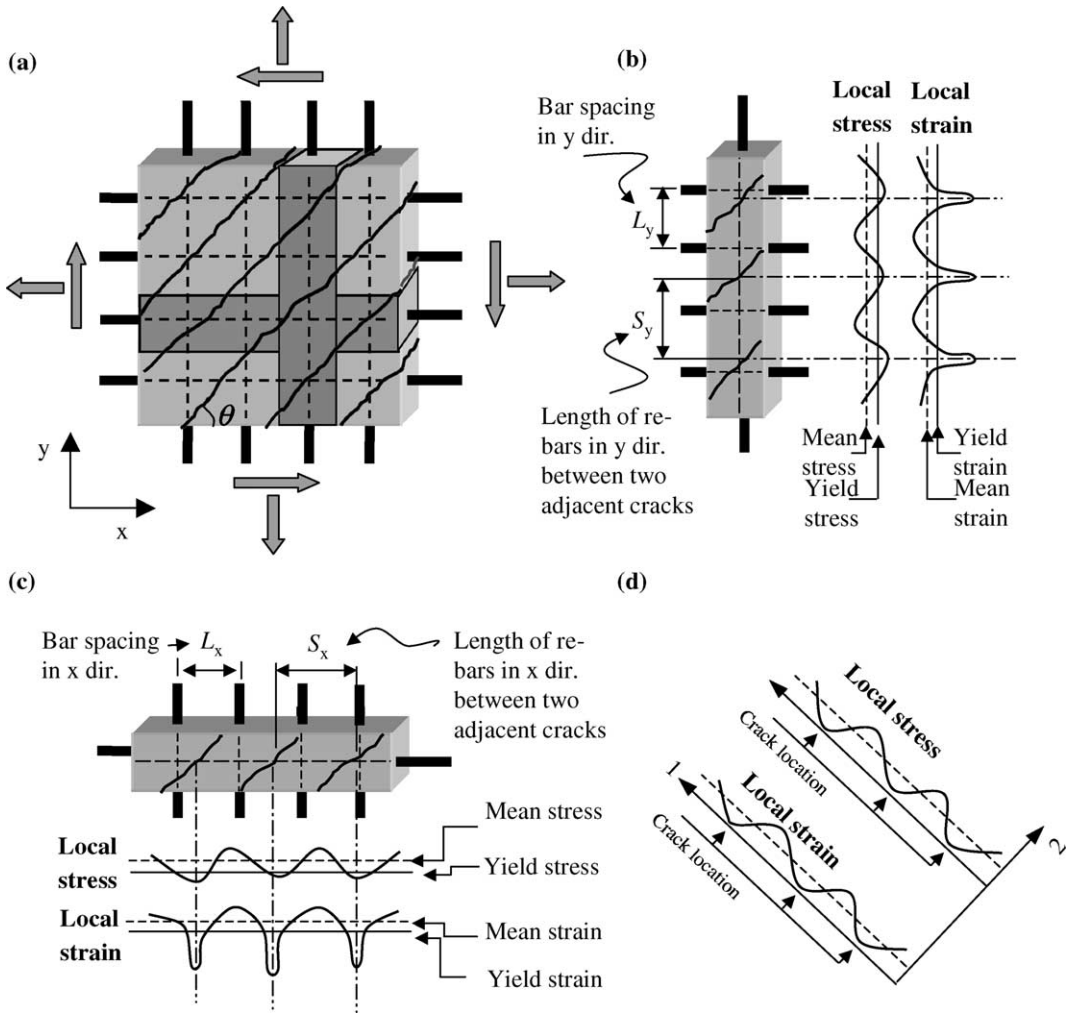

Fig. 3. Stress mobilized in cracked RC domain: (a) RC element subjected to in-plane stresses; (b) stress–strain along the re-bars in y direction; (c) stress–strain along the re-bars in x direction; (d) concrete stress–strain between cracks.

bond condition in two general groups: good bond condition and other bond conditions. The bond capacity for good bond condition is defined as

$$\tau_u = 0.1\sqrt{f'_c}, \quad \text{cold drawn wires}$$
$$\tau_u = 0.3\sqrt{f'_c}, \quad \text{hot rolled bars} \qquad (5)$$

where, f'_c is in MPa. In the case of other bond condition, the capacity is considered as half of the value in Eq. (5). It should be noted that the scatter of experimental results on bond-slip relation of plain bar is considerable, so definition of a general bond-slip model for plain bar without consideration to the real bond condition may not coincide with the real case. Bond condition effect however, will be examined in the subsequent sections. The CEB-FIP model code also cannot be used after yielding of reinforcing bars. In fact, the steel may yield before the local bond stress reaches the maximum capacity. In such a situation, just after yielding of reinforcement the local bond stress extensively reduces due to large slippage caused between reinforcing bars and concrete. In this work, no bond stress is assumed for post yielding of plain bars.

The bond performance near the crack plane may easily deteriorate due to splitting and crushing of concrete around the bar [15,16]. In order to consider this effect, the "bond deterioration zone" is considered beside the crack surface (L_b) as defined by Qureshi and Maekawa [16], which is a function of bar diameter (D_b).

Bond stress is assumed to linearly decrease from its maximum value (τ_{max}) attained at a distance L_b from the crack surface to half of this value ($\tau_{max}/2$) at a distance $L_b/2$ from the crack surface (Fig. 4). No bond stress is considered at a distance of $L_b/2$ from the crack surface (Fig. 4), as near the crack plane, the radial bond microcracks reach the surface of the crack plane and bond stress decreases, rapidly. Based on works of Shin [17], Qureshi and Maekawa [16] the bond deterioration zone can be considered as $5D_b$ from the crack surface when the reinforcing bar is perpendicular to cracks or pushing at right angles to the shear plane.

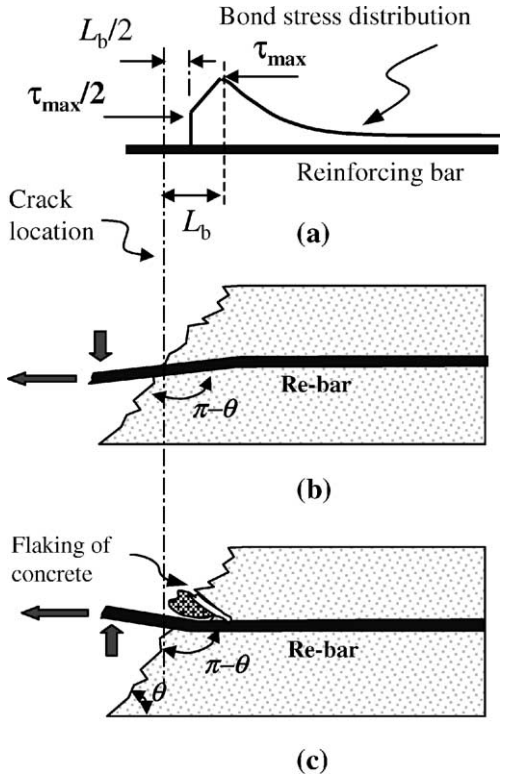

Fig. 4. Deterioration of bond close to the crack: (a) bond in deterioration zone; (b) bar pushing at right angle; (c) pushing to the less confined surface.

When the reinforcement is oblique to the shear plane and pushing against less confined free surface of the supporting concrete, due to flaking of concrete, both deterioration and curvature zone increase (Fig. 4). Qureshi [18] has shown that in such situations, the curvature zone increases up to $10D_b$ at a very large angle (close to 180°) between reinforcing bar and crack plane leading to increase the bond deterioration zone. In the computation for such a case, the linear interpolation is adopted as

$$L_b = 5D_b, \quad \text{pushing at right angle}$$
$$L_b = 5D_b\left(\frac{2(\pi-\theta)}{\pi}\right), \quad \text{pushing against free surface} \tag{6}$$

where, θ is crack angle.

In RC elements reinforced with welded wire mesh, also large amounts of stress transfer from the reinforcing bars to the concrete due to the pushing of wires against the supporting concrete. The concrete acts as a bearing support for transverse and longitudinal bars and prevents the slippage of reinforcing bars at welding points. The bearing stiffness and strength of concrete under action of reinforcing bars have been experimentally studied [19,20]. The foundation stiffness of bearing concrete in elastic range can be determined as [19]:

$$K = \frac{150f_c'0.85}{D_b}\left(\text{Unit}: \frac{\text{MPa}}{\text{mm}}\right) \tag{7}$$

where, D_b is diameter of reinforcing bar in mm and f_c' is cylindrical strength of concrete in MPa.

The bar is modeled as a beam resting on the elastic foundation. The deformation of steel bars placed in transverse direction (y), can be computed through solving the governing differential equation as

$$\frac{d^4\delta(y)}{dy^4} + \frac{KD_{by}}{E_{sy}I_{by}}\delta(y) = 0 \tag{8}$$

where, $\delta(y)$ is the deflection along the transverse bar, D_{by} is diameter of transverse bar and E_{sy} and I_{by} are the elastic modulus and moment of inertia of the bar section, respectively. The deformation of transverse bars at welding point equals the slippage of longitudinal bars at this point (Fig. 5) that is a boundary condition for solving the differential equation along the steel bars (Eq. (8)). So for each welding point, the total force transfer due to anchorage effect of transverse bars is computed as (exact solution):

$$F_{wy} = D_{by}\int_{L_y} f_w(y)\,dy \tag{9}$$

where, $f_w(y)$ is bearing stress along the transverse bar equal to $K\delta(y)$ and L_y is the spacing of longitudinal bars (Fig. 3). However, when more than one reinforcing bars push against concrete (RC elements with distributed bars), the deflection of reinforcing bars between two adjacent welding points can be assumed on average equal to the bar slippage at welding point (Fig. 5). So, for such situations, the total stress transfer from transverse wires in each welding point is expressed as (approximate solution):

$$F_{wy} = KD_{by}L_yS_b(x_w) \tag{10}$$

where, $S_b(x_w)$ is axial slippage of longitudinal bar at the welding point location (Fig. 5). In the same way, the force transfer due to anchorage effect of longitudinal wires can be computed.

Based on local analysis along the reinforcing bars using governing strain compatibility and equilibrium of stresses, the stress and strain profile along the reinforcing bars can be determined which demands proper simulation of stress transfer mechanism as well as length of reinforcing bars along which the stresses of reinforcements transfer to the concrete (see Fig. 3). The tensile stress transfer from reinforcing bars to the concrete is the main mechanism that controls the crack development in RC domain, crack spacing and width and also the spatial average behavior of re-bars and concrete.

For any given average re-bar strain, the profile of strain and stress along the reinforcement can be computed based on the bond stress distribution along the

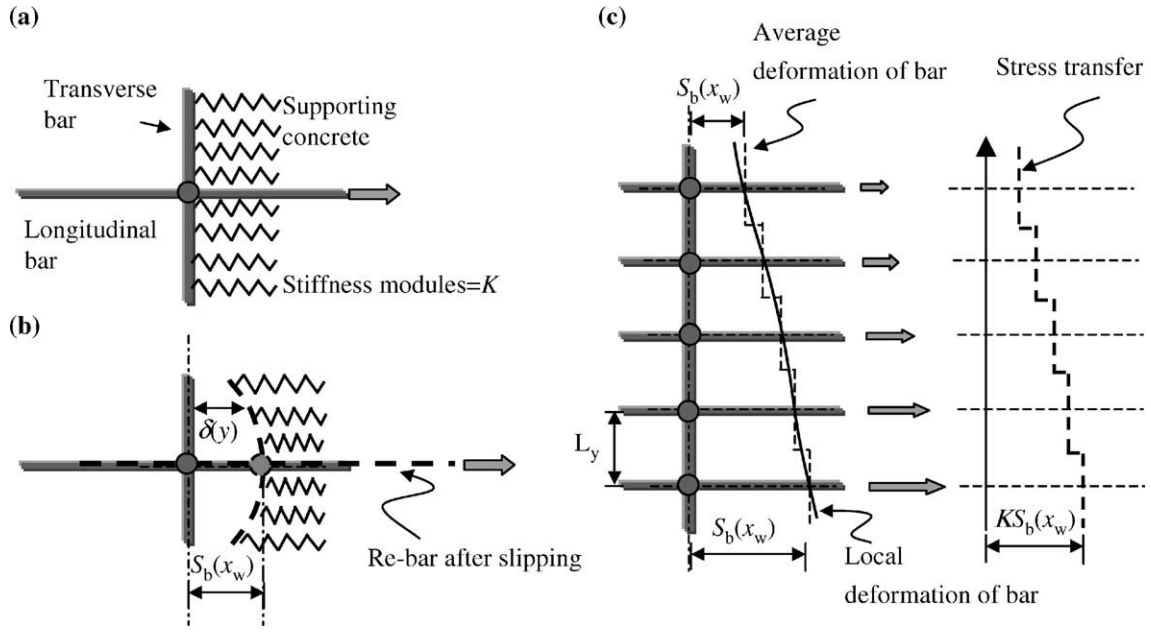

Fig. 5. Anchorage effect of transverse and longitudinal reinforcing bars: (a) single longitudinal reinforcing bar; (b) deformation of single reinforcing bar at welding point; (c) deformation of distributed bars under general displacement.

reinforcing bar and stress transfer due to anchorage effect of bars (as explained before). If average crack spacing is known, the average length of longitudinal and transverse bars between two adjacent cracks can be computed as

$$S_x = \frac{S_{xy}}{\sin\theta} \tag{11a}$$

$$S_y = \frac{S_{xy}}{\cos\theta} \tag{11b}$$

where, S_{xy} is average crack spacing and S_x, S_y are average length of reinforcing bars between adjacent cracks in x and y directions, respectively.

The length of reinforcing bar between two adjacent cracks is divided into many small segments. Satisfying the equilibrium conditions on one segment, the following equilibrium equation is derived (Fig. 6):

$$\frac{\Delta\sigma}{\Delta l} = \frac{\pi D_b}{A_{sb}}\bar{\tau} \tag{12}$$

where, $\Delta\sigma/\Delta l$ is gradient of steel stress along the bar (x or y coordinate axis), A_{sb} is cross section area of reinforcing bars and $\bar{\tau}$ is the average bond stress along the segment. To compute the stress transfer due to bond and anchorage effect of bars in the same manner, the total stress transfer from the anchorage effect of reinforcing

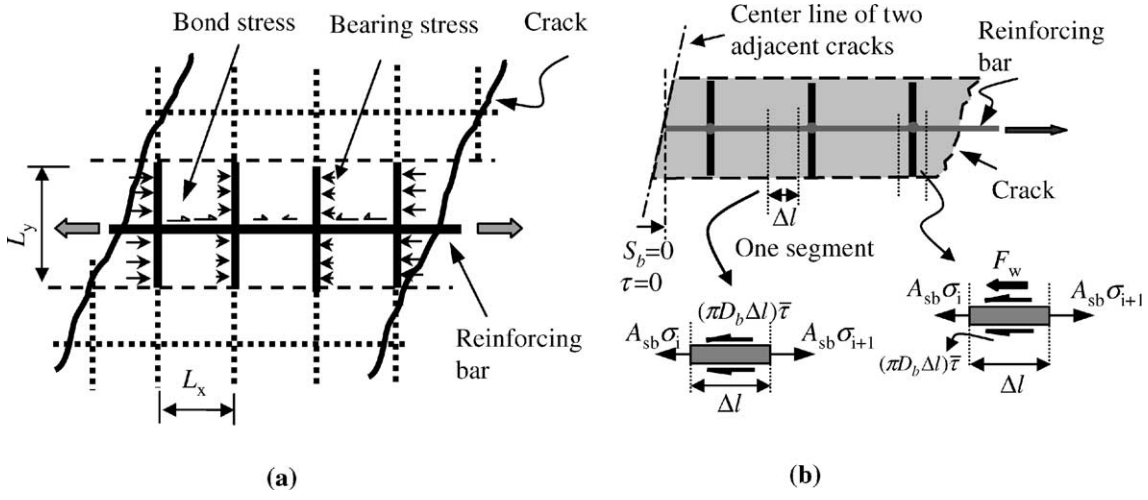

Fig. 6. Tensile stress transfer to the concrete through bond and anchorage effect: (a) bond and bearing stress; (b) equilibrium in small segment.

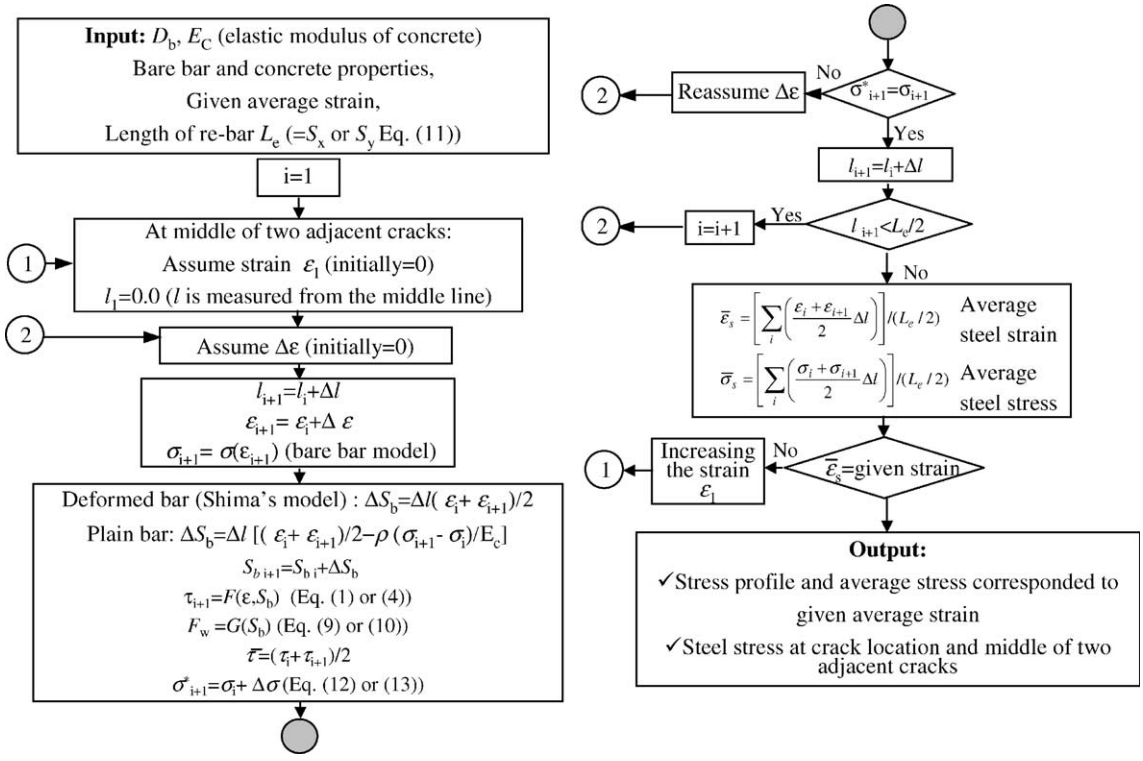

Fig. 7. Flowchart of computing stress profile and average stress along the reinforcing bars.

bars is added to the bond stress value for the segments at welding points (Fig. 6) as

$$\frac{\Delta\sigma}{\Delta l}=\frac{\pi D_b}{A_{sb}}\bar{\tau}+\frac{F_w}{\Delta l A_{sb}} \tag{13}$$

The bond stress and the slip at the midway between two adjacent cracks are zero, which are the boundary conditions for the first finite segment. Assuming strain value at the middle of two cracks, the stress and strain profiles are computed by solving the equilibrium and slip compatibility equations, segment by segment along the reinforcing bar.

Starting from the first segment at midway between two adjacent cracks and assuming the strain increment, the stress and the slip value at the other side of the segment and consequently the bond stress are computed. Increasing the strain increment (compared to the previous step), an iterative procedure is done until the obtained stress value satisfies the equilibrium condition (Eq. (12) or (13)). The computed strain and slip for the

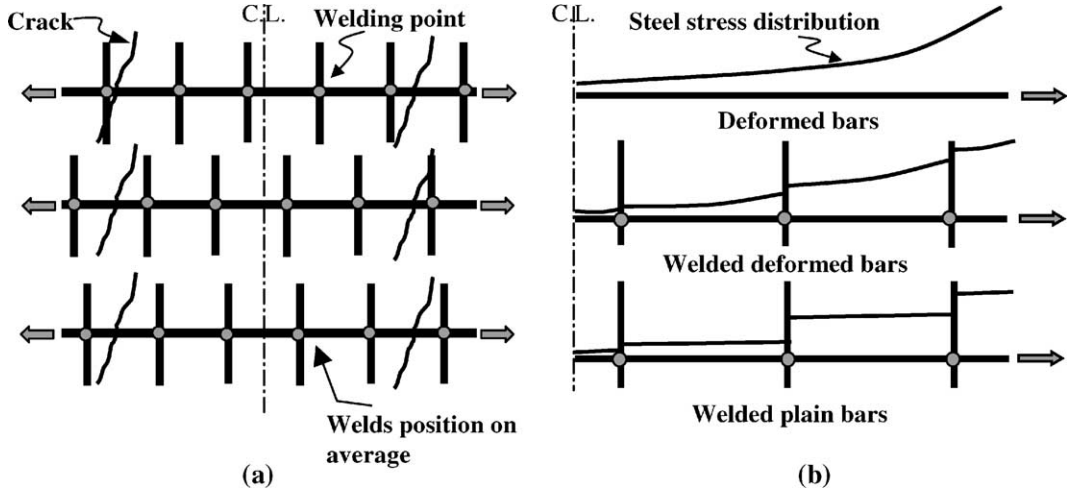

Fig. 8. Crack location and distribution of stress: (a) welding point location; (b) steel stress distribution along the bar.

first segment will be the boundary condition for the next segment. A similar computation procedure is followed to attain the stress and strain profile along the reinforcing bar (see flowchart shown in Fig. 7).

The welding points may have any arbitrary location along the length of reinforcing bars between two adjacent cracks, but on average it can be assumed to be symmetric between cracks (Fig. 8(a)). The steel stress distribution along the reinforcing bars for three different cases: conventional deformed bars, welded deformed bars and welded plain bars, schematically has been shown in Fig. 8(b). In the normal case the stress along the reinforcing bars between two adjacent cracks gradually decreases along the reinforcing bar, but in the case of welded bars, large amounts of stress transfer at welding points leading to drop of steel stress in these points. The steel stress between two adjacent welding points depends on the bond condition of reinforcing bars. Deformed bars show larger amounts of stress transferring to the concrete between two adjacent welding points.

4. Tensile stress transfer into the concrete

The local stresses of cracked concrete and reinforcing bars at crack surface are shown in Fig. 9(a). These local stresses statically are equivalent with applied stresses. So, writing equilibrium equations in direction normal to cracks we have:

$$\sigma_d + \sigma_{br} = \sigma_x \sin^2\theta + 2\tau_{xy}\sin\theta\cos\theta + \sigma_y\cos^2\theta - \rho_x f_{crx}\sin^2\theta - \rho_y f_{cry}\cos^2\theta \quad (14)$$

where, ρ_x, ρ_y, are reinforcement ratios in x and y directions, respectively. σ_x, σ_y, are applied stresses in x and y directions and τ_{xy} is applied shear stress. σ_d is dilatancy stress normal to crack and σ_{br} is the bridging stress of cracked concrete (the tensile stress is considered positive), f_{crx} and f_{cry} are stresses of reinforcing bars at crack plane in x and y directions, respectively and θ is the crack angle. Also, the equilibrium equation can be written based on the average stresses of concrete and reinforcements (Fig. 9(b)) as

$$\sigma_1 = \sigma_x \sin^2\theta + 2\tau_{xy}\sin\theta\cos\theta + \sigma_y\cos^2\theta - \rho_x f_{avx} \times \sin^2\theta - \rho_y f_{avy}\cos^2\theta \quad (15)$$

where σ_1 is the average tensile stress transfer to the concrete (tension stiffening), f_{avx} and f_{avy} are average stresses of reinforcing bars in x and y directions, respectively. By comparison of the two above equations, total average tensile stress transfer to the cracked concrete (tension stiffening) can be formulated as

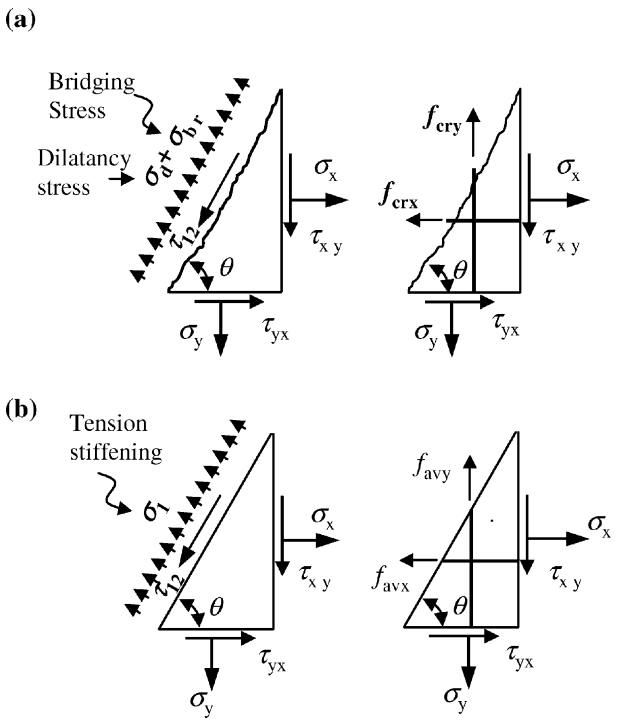

Fig. 9. Stress state of cracked concrete and reinforcing bars: (a) local state; (b) average state.

$$\sigma_1 = \rho_x(f_{crx} - f_{avx})\sin^2\theta + \rho_y(f_{cry} - f_{avy})\cos^2\theta + \sigma_d + \sigma_{br} \quad (16)$$

Therefore, the tension stiffening of cracked concrete is expressed as the summation of tensile stress transferred along the reinforcing bars (σ_t), bridging stress (σ_{br}) and dilatancy stress (σ_d). Eq. (16) shows the dependency of tension stiffening to the crack inclination and micro characteristics of stress transfer to the concrete. Knowing the crack width and slip of crack surfaces, the bridging stress and dilatancy stress of cracked concrete can also be determined based on the material relations of cracked concrete as described following.

5. Other material relations

5.1. Bridging stress normal to cracks

When crack is localized in concrete domain, some residual tensile stresses transfer normal to cracks due to interlocking of crack surfaces. As a result the tensile stress at crack plane does not drop to zero and concrete shows softening behavior after cracking. Actually, in reinforced concrete with an ordinary reinforcement ratio, the tension softening of concrete can be neglected compared to the bond stress transfer to concrete. However, in lightly reinforced concrete element this phenomenon must not be neglected [11,21].

The tension-softening model is usually expressed as a relationship between crack width and bridging stress. Here Ushida's model [22] is adopted for analysis:

$$\sigma_{br} = f_t\left[1 + 0.5\omega_{cr}\left(\frac{f_t}{G_f}\right)\right]^{-3} \quad (17)$$

where, σ_{br} is bridging stress transfer across the crack, f_t is tensile strength of concrete, ω_{cr} is crack width and G_f is fracture energy of plain concrete.

5.2. Concrete in compression

The elasto-plastic and fracture model proposed by Maekawa and Okamura [23], that expressed the stress–strain relationship of concrete under uniaxial compression and also multi axial stresses, is adopted in this work. The model expresses the relationship between equivalent strain and stress based on the initial elastic modulus, the fracture parameter and the equivalent plastic strain. The reduction of compressive stiffness after propagation of cracks in the model is mathematically considered by modifying the fracture parameter as a function of strain perpendicular to the crack plane (Fig. 10). The model has been expressed and widely used elsewhere, which can be referred to for details [9,23].

5.3. Shear and dilatancy stresses transfer across cracks

Two main mechanisms of shear transfer across cracks are interaction between the rough surfaces of the crack and dowel action due to curvature of reinforcing bar at the crack plane. As the shear displacement takes place in crack interface, enforcement of the aggregate particles to each other, with consequential tendency for widening of cracks (dilatancy), will occur. This crack widening increases the axial stress in reinforcing bar. At the same time, shear displacement causes the flexural effect in reinforcing bar, which consequently produces the shear stress in some parts along the reinforcement close to crack interface. Qureshi and Maekawa [15] experimentally studied the dowel action and its contribution on shear stress transfer across cracks. They concluded that the dowel action and kinking of reinforcing bars at crack plane have minor effect on the structural behavior compared to the shear stress transfer due to the aggregate interlock. For simplification of the proposed method, this effect is neglected in this work.

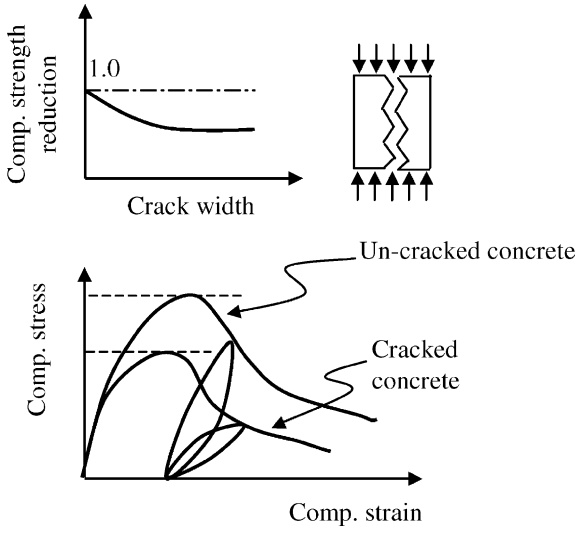

Fig. 10. Stress–strain relationship of cracked and un-cracked concrete in compression.

The overall stress transfer system in reinforcing bar and concrete strictly controls the crack width and slip in RC member, which actually affects the shear transfer ability of crack plane. The aggregate interlock model used here is based on the 'universal stress transfer model' proposed by Bujadham and Maekawa [24], which has large applicability and is verified by extensive experimental results under different monotonic and cyclic loading paths. The framework of the model is based on the original contact density model [25] with consideration of all characteristics of concrete stress transfer behavior, e.g. microscopic friction on aggregate particles, anisotropic plasticity of contact stress and fracturing of contact units. Details of the model can be found in Bujadham and Maekawa [24].

6. Local analysis of RC elements and averaging

Using the equilibrium equations, the applied stress components can be expressed based on the stresses of cracked concrete and those of reinforcing bars. Replacing the local normal stress of concrete and also reinforcing bar stresses at crack plane by average tensile stress of concrete and reinforcing bar, the equilibrium equations can be expressed as

$$\sigma_x = (\sigma_t + \sigma_d + \sigma_{br})\sin^2\theta + \sigma_2\cos^2_\theta + 2\tau_{12} \times \sin\theta\cos\theta + \rho_x f_{avx} \quad (18)$$

$$\sigma_y = (\sigma_t + \sigma_d + \sigma_{br})\cos^2\theta + \sigma_2\sin^2\theta - 2\tau_{12} \times \sin\theta\cos\theta + \rho_y f_{avy} \quad (19)$$

$$\tau_{xy} = (\sigma_t + \sigma_d + \sigma_{br} - \sigma_2)\sin\theta\cos\theta + \tau_{12}(\cos^2\theta - \sin^2\theta) \quad (20)$$

where, σ_x, σ_y are applied normal stresses in x and y directions respectively, and τ_{xy} is applied shear stress in x–y direction. Sign convention is considered, as shown in Fig. 2.

Using strain compatibility relationship, the strains in global direction (x–y coordinate system) can be expressed in terms of three components of strain $(\varepsilon_1, \varepsilon_2, \gamma_{12})$ in local axes of cracked concrete:

$$\varepsilon_x = \varepsilon_1 \sin^2\theta + \varepsilon_2 \cos^2\theta + \gamma_{12} \sin\theta\cos\theta \quad (21)$$

$$\varepsilon_y = \varepsilon_1 \cos^2\theta + \varepsilon_2 \sin^2\theta - \gamma_{12} \sin\theta\cos\theta \quad (22)$$

$$\gamma_{xy} = 2(\varepsilon_1 - \varepsilon_2)\sin\theta\cos\theta + \gamma_{12}(\cos^2\theta - \sin^2\theta) \quad (23)$$

All quantities in right hand sides of equilibrium equations (Eqs. (18)–(20)) can be computed by local analysis along the reinforcing bars and across cracks. Considering local strains of cracked concrete as primary unknown parameters, the average steel strains are calculated. Knowing the crack spacing and average strain of reinforcing bars, the steel stress and strain profile and consequently the average stresses of reinforcements and stress mobilized in concrete are computed (Eq. (16)). Average crack width (ω_{cr}) and shear slip (δ_{cr}) are obtained by multiplication of tensile strain and shear strain of cracked concrete by crack spacing:

$$\omega_{cr} = \varepsilon_1 \times S_{xy} \quad (24)$$

$$\delta_{cr} = \gamma_{12} \times S_{xy} \quad (25)$$

The elastic deformations of concrete between two adjacent cracks are neglected, as they are very minor compared to crack opening and sliding. Therefore, in each loading step, the crack width and slip and consequently the local stress of cracked concrete (bridging stress, shear and dilatancy stress), can be computed. The computed steel and concrete stresses should satisfy the equilibrium conditions (Eqs. (18)–(20)). So, for any given applied stresses, the unknown average strains can be determined in an iterative way.

The crack spacing is initially considered equal to the length of elements normal to the crack direction. Satisfying the equilibrium conditions at centerline between cracks we have:

$$\sigma_{C.L.} = \text{resultant stress normal to C.L.} - \lfloor \rho_x f_{mid\text{-}x} \sin^2\theta + \rho_y f_{mid\text{-}y} \cos^2\theta \rfloor \quad (26)$$

where, $f_{mid\text{-}x}$ and $f_{mid\text{-}y}$ are steel stresses between two adjacent cracks (Fig. 11). In each loading step the maximum local stress of concrete is checked. When the maximum local concrete stress exceeds the tensile strength of concrete, a new crack in the middle of initial cracks is introduced and computation is carried out with new crack spacing. It should be noted that because of non-uniformity of concrete, the location of new cracking is not necessarily in the middle of two previous cracks, so the calculated crack spacing could be assumed as average crack spacing.

The procedure is followed until cracks reach a stabilized state which takes place either after yielding of reinforcing bars or when the crack spacing becomes so small that the bond stress transfer to concrete is not sufficient enough for any further cracking. Since, in reality, it is not possible for two cracks to occur simultaneously, as experimentally shown by Goto [15], Rizkalla and Hwang [26], in each cracking state it is assumed that just one new crack generates in RC domain, and the average crack spacing is computed as

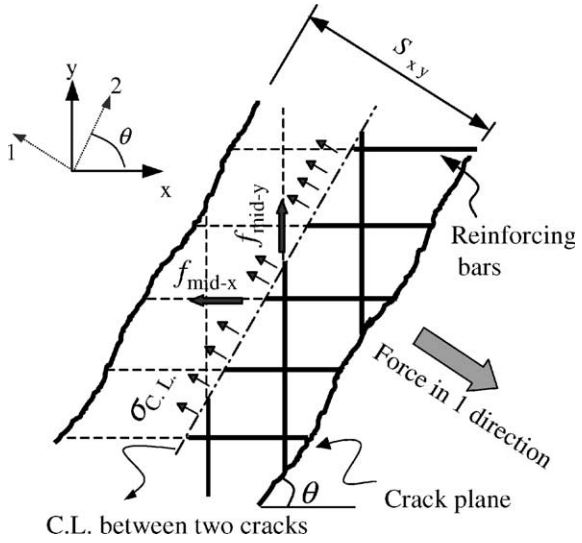

Fig. 11. Local stress at centerline between two adjacent cracks.

$$S_{xy} = \frac{S_0}{N_{cr}} \quad (27)$$

where, S_0 is initial crack spacing (length of specimen normal to crack direction) and N_{cr} is number of generated cracks. It is assumed herein that the cracks form in uniform manner and the direction of cracks remain fixed during loading. In fact, large anisotropy of steel forces at crack location sometimes tends to the rotation of crack from its initial orientation that results on failure of the panel [27]. This phenomenon, which depends on the loading condition and reinforcement ratio, can also be investigated through micro mechanism of load transferring in RC domain, which is not the objective of this work.

The computation procedure can be summarized as follows (see also flowchart in Fig. 12):

Step 1: The tensile strain of cracked concrete (ε_1), concrete strain in crack direction (ε_2) and shear strain of cracked concrete (γ_{12}) are assumed as primary unknown parameters.

Step 2: Using Eqs. (24) and (25), the crack width and slip are computed. The crack spacing in the last step is used in computation. The initial crack spacing is considered as the length of specimen.

Step 3: Using compatibility equations (Eqs. (21)–(23)) the average strain of reinforcing bars and global strains of RC elements are computed.

Step 4: Computing the length of reinforcing bars between two adjacent cracks (Eq. 11) and solving the governing equation along the length of reinforcing bars (Eqs. (12) and (13)), the stress distribution along the reinforcing bars and also

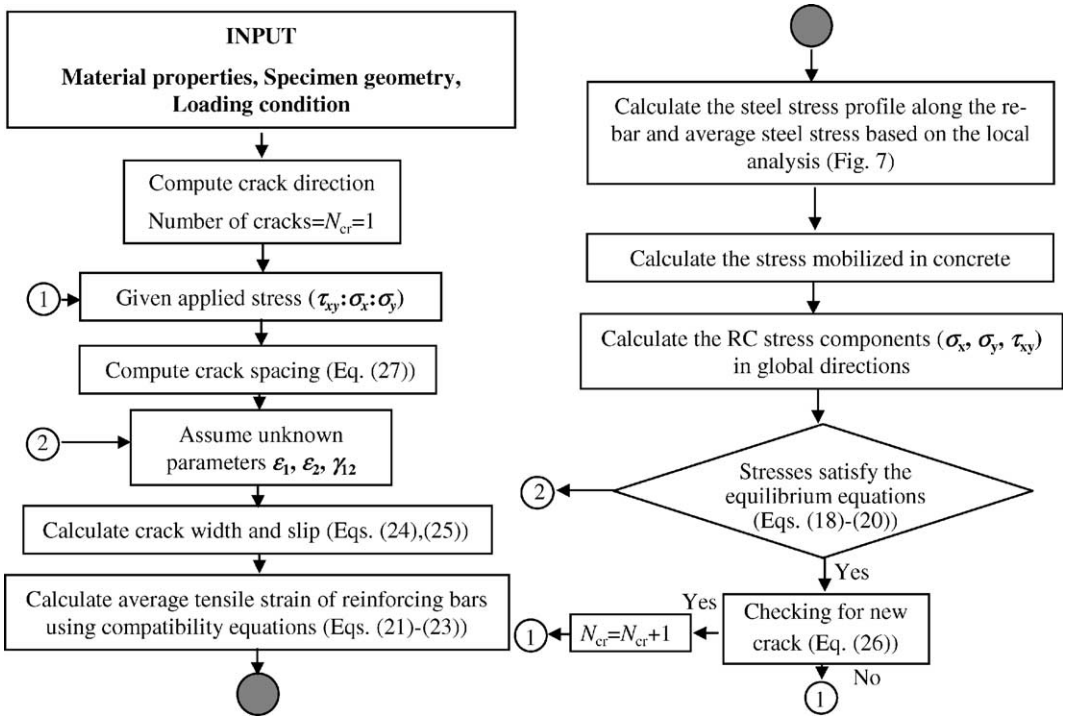

Fig. 12. Flowchart of computation.

average tensile stress of reinforcing bars in any steel direction is computed.

Step 5: The stress components of concrete are computed as explained in previous sections. The shear stress (τ_{12}) and dilatancy stress (σ_d) are computed based on crack width and shear slip obtained in step 2. The tensile stress mobilized in cracked concrete (tension stiffening) is computed using Eq. (16) based on the local stress of reinforcing bars computed in step 4.

Step 6: Steps 1 through 5 are repeated until the equilibrium in Eqs. (18)–(20) is obtained (using an iterative solution method such as Newton–Raphson iterative method). In this situation the total stresses of RC elements in global direction are computed.

Step 7: The state of stresses between two adjacent cracks is checked, if the tensile stress exceeds tensile strength of concrete, the new crack is introduced, and the computation is carried out with new crack spacing.

Step 8: The computation (step 1–7) is carried out for any loading step.

7. Experimental verification

7.1. RC panels subjected to in-plane stresses

For verification of the proposed analytical method, a comparison with experimental results on RC panels was carried out. The series of experimental results involving reinforced concrete panel specimens subjected to in-plane stresses conducted by Vecchio and Collins [4] were selected. The details of specimens and loading conditions are listed in Table 1. All specimens have been

Table 1
Specimen details and loading conditions

Panel	Concrete					Reinforcing bars					Loading, $\tau_{xy} : \sigma_x : \sigma_y$
	f'_c (MPa)	$\varepsilon_c \times 10^{-3}$	ρ_x (%)	F_{y-x} (MPa)	D_{bx} (mm)	L_x (mm)	ρ_y (%)	F_{y-y} (MPa)	D_{by} (mm)	L_y (mm)	
PV1	34.5	−2.20	1.79	483	6.35	50	1.68	483	6.35	54	1:0:0
PV3	26.6	−2.30	0.483	662	3.3	50	0.483	662	3.3	50	1:0:0
PV5	28.3	−2.50	0.742	621	5.79	100	0.742	621	5.79	100	1:0:0
PV9	11.6	−2.80	1.79	455	6.35	50	1.79	455	6.35	50	1:0:0
PV11	15.6	−2.60	1.79	235	6.35	50	1.31	235	5.44	50	1:0:0
PV14	20.4	−2.23	1.79	455	6.35	50	1.79	455	6.35	50	1:0:0

orthogonally reinforced with welded wire mesh made from plain bars.

The tensile strength of concrete in RC panels, which is affected by many factors such as drying shrinkage, affects the behavior of panels. As these panels were tested at early age (6–10 days), the data corresponding to the tensile strength of concrete shows large scatter (as reported in [4]) that cannot be predicted by simple expression (for example proposed formula by ACI [28]). Therefore, in the analysis, the tensile strength of concrete was considered based on the reported cracking stress.

The bond stress was modeled based on the CEB-FIP model code. The bearing stiffness in Eq. (7) was adapted in analysis. It should be noted that due to the cracking nature of concrete, the stresses of supporting concrete are small and the supporting concrete can be considered to behave elastically. Maximum bearing stress computed in the analysis was about 9 MPa (panel PV3) that is about $0.3f'_c$. However it should be considered that the bearing strength is higher than compression strength [20]. The comparisons between experiment and analytical results, in terms of shear stress–strain relationship, are illustrated in Fig. 13. Generally, analytical method agrees well with the experimental results.

As in the proposed method, all stress components mobilized in RC domain are obtained in terms of micro characteristics of stress transfer and local response of components, the average stress–strain relationship of reinforcing bars and cracked concrete both normal and across cracks can be computed and the effect of macro characteristics of element (type, size and arrangement of reinforcing bars) and micro characteristics of stress transfer (bond condition, aggregate interlock) on the cracking response and spatially averaged stress–strain relationship of components, can be investigated.

In Fig. 14 the computed tensile stress transfer through cracked concrete (normalized tension stiffening), that is the summation of tensile stress transfer due to bond, bearing stress of wires, bridging stress and dilatancy stress are compared with the experimental results and the Okamura–Maekawa model [9]. It should be noted that the tension stiffening based on experimental results is valid until yielding of reinforcement as the tension stiffening after yielding of reinforcement can be computed if the average yielding of reinforcement is measured in the experiment. Good agreement between experiment and computed tensile stress of cracked concrete is obvious in Fig. 14.

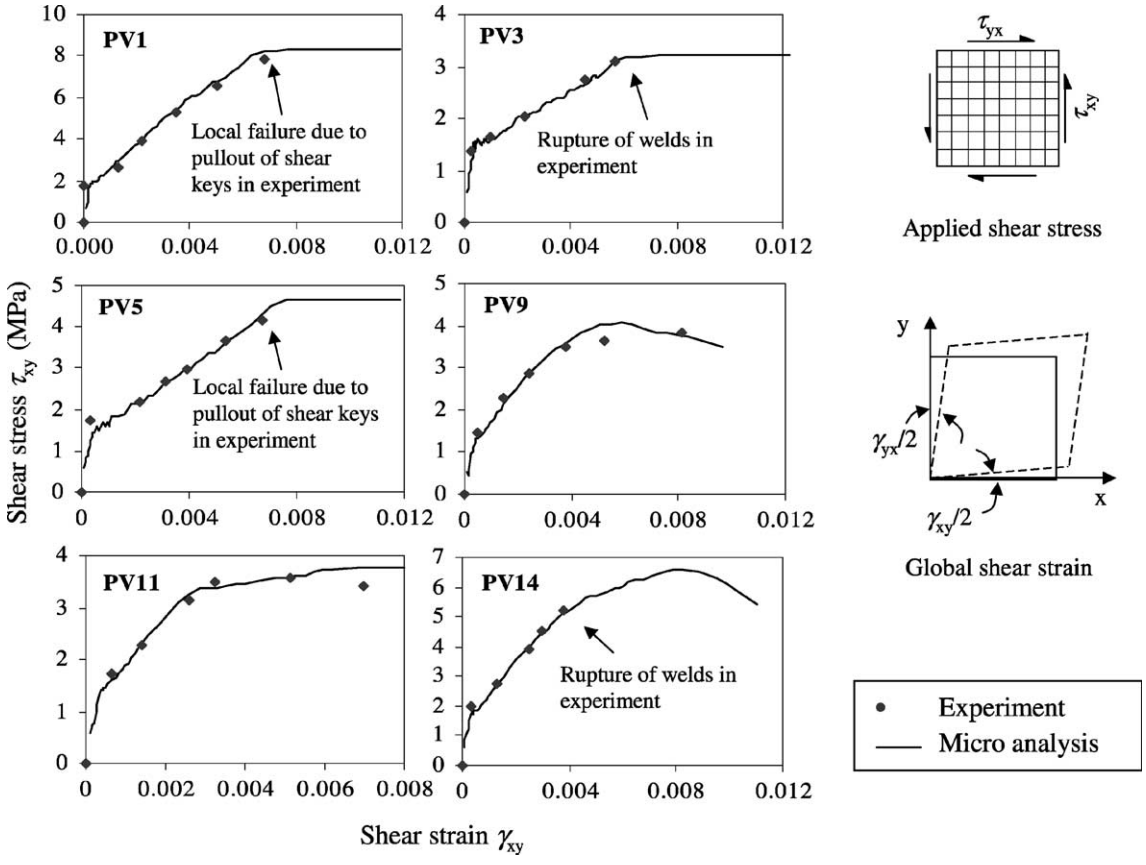

Fig. 13. Comparison of computed shear stress–strain relationship.

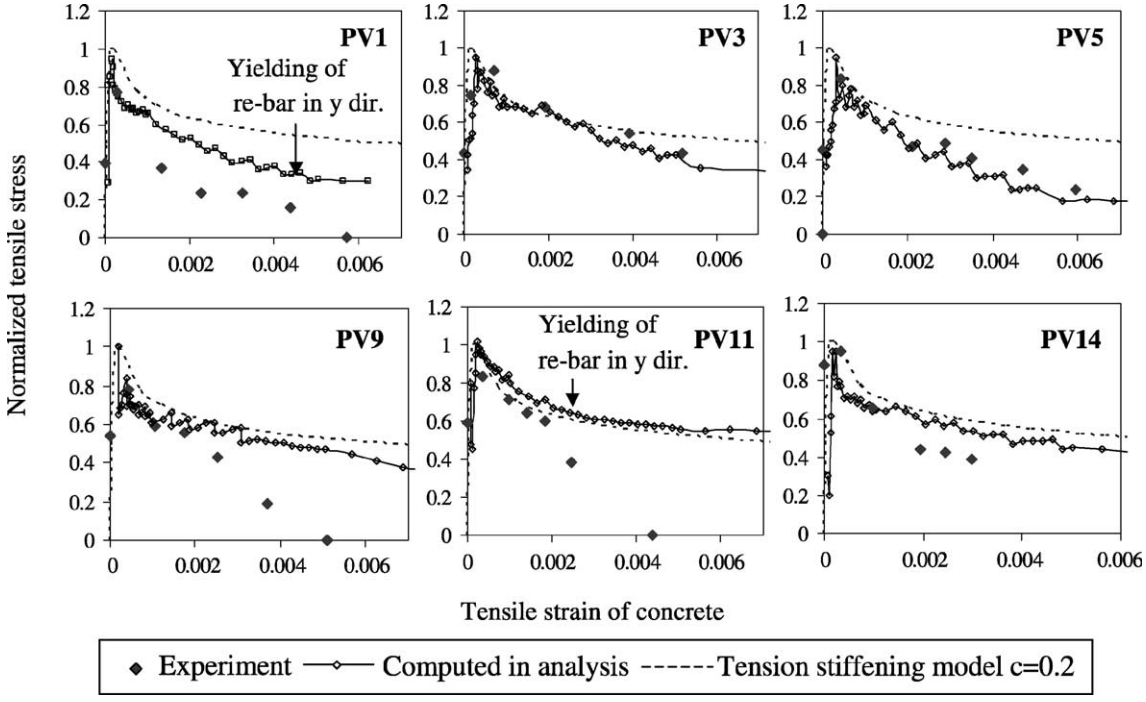

Fig. 14. Comparison of computed tension stiffening, experiment and model.

7.2. Cracking response of RC member subjected to direct tension

Lee et al. [2] experimentally investigated the effect of type and spacing of welded wires on crack spacing and crack width of RC members in direct tension. The tested specimens had a 700 mm length with 105×55 mm cross-section.

All specimens longitudinally reinforced with one reinforcing bar had a diameter of 12 mm and transversely reinforced with 10 mm bars. Two types of reinforcing bars; smooth bar and deformed bar were examined in the experiment. The bond stress-slip for both types of reinforcing bars was measured and reported in their work.

The proposed procedure was carried out for crack analysis of the specimens. The reported bond-slip for deformed and smooth bar was used in the analysis. The tensile stress transfer through anchorage effect of transverse wires was computed through solving the governing deferential equation (Eq. (8) for single bar—Fig. 5).

Comparison between average crack spacing in experiment and analysis is shown in Fig. 15. The computed crack spacing shows acceptable agreement with the experimental results. In fact the small length of specimens cannot represent well the average response of element as only a few numbers of cracks are developed in this case. The existence of transverse wires provides a weaker cross section by reducing the effective concrete area, leading to increase in the potential for cracking in those points. So, minimum and maximum crack spacing can be considered to be a factor of spacing of transverse wires that are close to the average crack spacing.

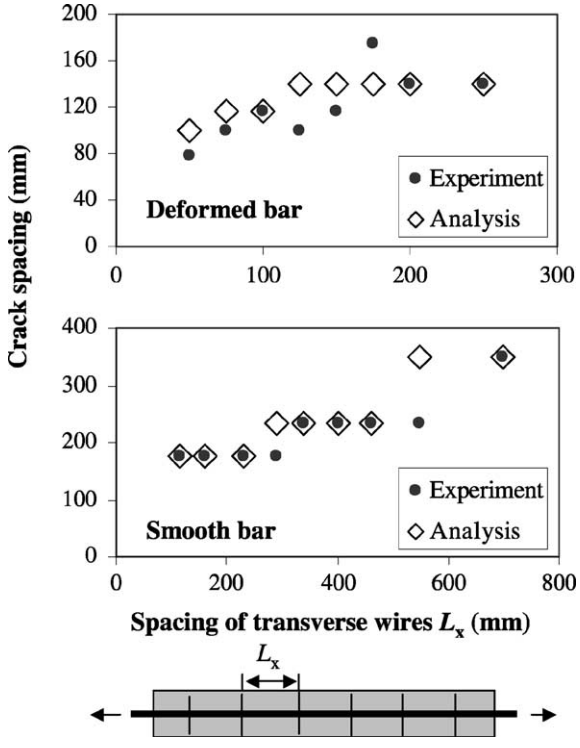

Fig. 15. Comparison of average crack spacing in experiment and analysis.

8. Effect of type and arrangement of wires on cracking response

Using proposed micro computational method, effect of bond performance, type and arrangement of reinforcing bars on cracking behavior of RC elements reinforced with welded wire mesh, can be investigated through parametric study. As it was described in previous sections, the bond between reinforcing bars and concrete is the main mechanism affecting the post cracking behavior of RC elements reinforced with deformed bar. However, in the case of RC elements reinforced with welded wire mesh, large amounts of tensile stress are transferred to the concrete due to anchorage effect of bars that is supposed to have significant effects on the cracking response of RC elements.

Two panels PV3 and PV5 were re-analyzed considering different bond conditions: welded deformed bars, welded plain bars and welded wires without any bond stress. Normalized tension stiffening models are compared in Fig. 16. It can be seen that the bond between concrete and reinforcing bars has minor effect on post cracking response of these panels. But one difference between these two panels is the wire spacing (50 mm in PV3 and 100 mm in PV5) that resulted different post cracking tensile stress for these two panels (see Fig. 14).

Fig. 17 illustrates the effect of wire spacing on the shear stress–strain relationship of panel PV3. The wire spacing was altered by the adjustment of wire diameter. Analysis was done with the same bond conditions (plain bars). It is shown that wire spacing has a large effect in tension stiffening and post cracking stiffness of elements. In small wire spacing, the tension stiffening is mainly controlled by anchorage effect of wires and bond between concrete and reinforcement has minor effect on the cracking response. The tension stiffening of welded wire mesh increases by reducing the wire spacing.

Generally, due to the large contribution of anchorage effect on the tension stiffening, it can be concluded that the tension stiffening of welded wire mesh is higher than that of deformed bars (for small wire spacing), but it should be noted that, when cracking is not perpendicular to the re-bars, due to non-equality of tensile strain of concrete and reinforcements (compatibility conditions), even though the same tensile stress transfers to the concrete, the average concrete strain corresponded to this stress is higher than steel strain which tends to have a higher tension stiffening compared to the direct tension case. In Fig. 18 the computed tension stiffening for panel PV11, with welded wire mesh (experiment) and with deformed bar is compared. The higher tension stiffening for welded wire mesh is obvious. Also, the computed tension stiffening for panel with the same geometry and reinforcement as panel PV11 but under direct tension is shown in the same figure that shows different tension stiffening compared to the pure shear

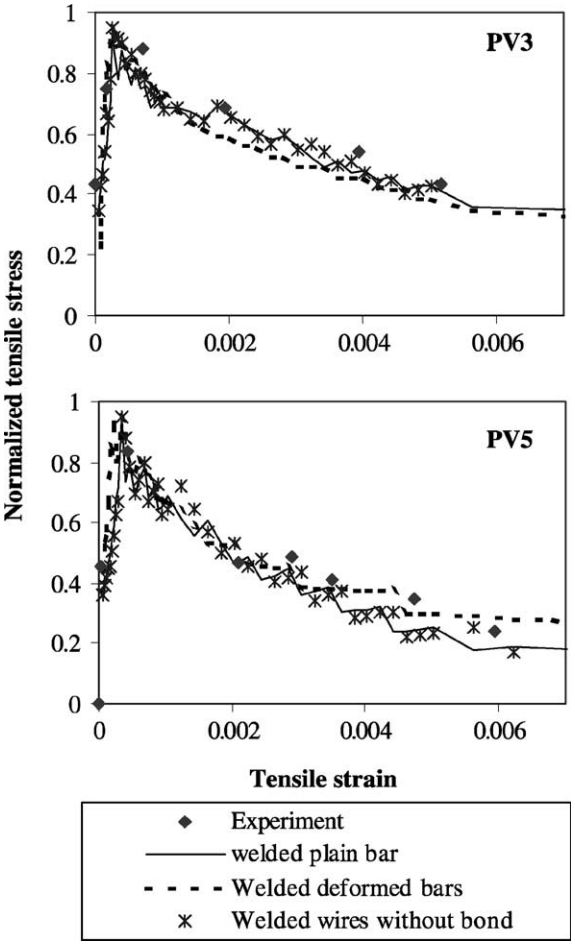

Fig. 16. Effect of bond on tension stiffening of welded wire mesh.

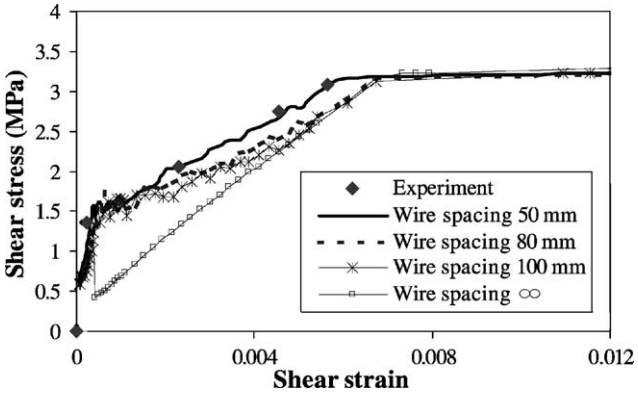

Fig. 17. Effect of wire spacing on average response of panel PV3.

case. Fig. 19 shows the average response of RC elements in direct tension with different wire spacing. In this case, the ultimate average strain is defined as the average strain at which the local steel stress reaches a certain ultimate stress (for example cutting of welds). It can be seen that ultimate average strain decreases (lower duc-

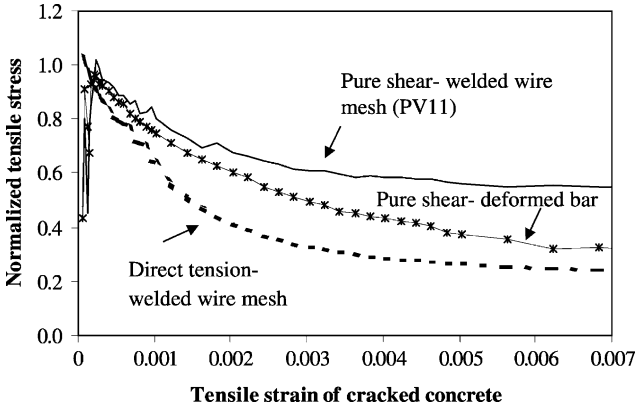

Fig. 18. Effect of type and loading condition on tension stiffening.

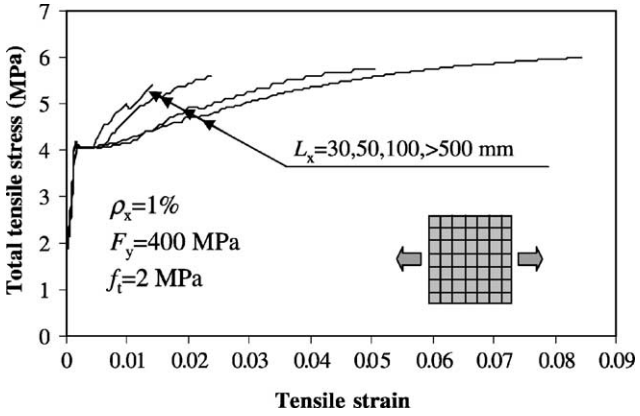

Fig. 19. Tensile response of RC elements with different wire spacing.

tility) with the decrease of wire spacing. For the case of small wire spacing, large amounts of steel stress are transferred to the surrounding concrete, and as a result steel stress at crack location reaches to the ultimate strength in lower average strain.

The effect of wire spacing and type of reinforcement on the crack spacing also was analytically examined. The parametric study (Fig. 20) shows that crack spacing for small wire mesh does not depend on the type of reinforcing bars, however, for large wire spacing the bond stress is the main mechanism that controls the spacing of cracks. The variations of crack spacing ratio for different types of reinforcing bars (crack spacing in RC elements reinforced with smooth bar/crack spacing in RC element reinforced with deformed bar) versus ratio of wire spacing to bar diameter (L/D_b, $L = L_x$ or L_y) are shown in Fig. 21. Two different reinforcement ratios have been examined. This figure indicates for L/D_b less than 20, the crack spacing is mainly governed by the anchorage effect of reinforcing bars and is independent on the type of reinforcements.

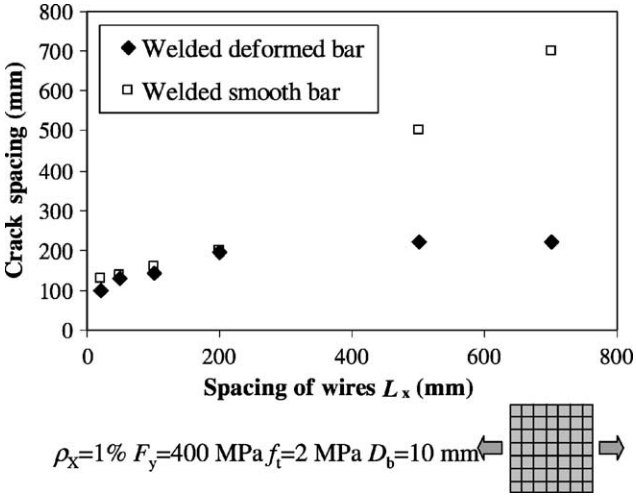

Fig. 20. Effect of type and spacing of wires on crack spacing.

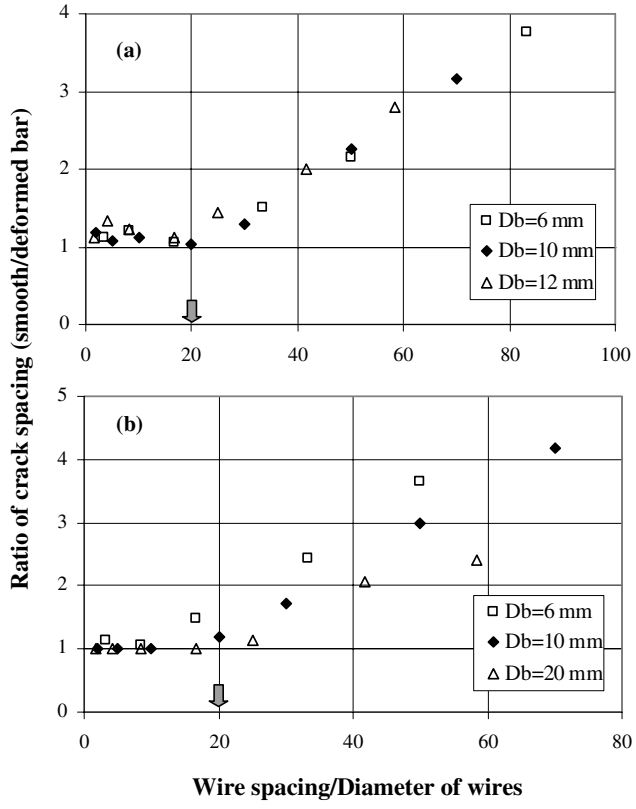

Fig. 21. Ratio of crack spacing versus L/D_b: (a) $\rho = 1\%$; (b) $\rho = 2\%$.

9. Conclusion

New methodology has been developed and used for analysis of RC membrane elements reinforced with welded wire mesh based on the micro mechanism of stress transfer in cracked RC domain. Unlike the smeared crack model that the spatially averaged behavior of material (constitutive models) is used in

the analysis, in the described model, the response of element is computed based on the local stress–strain behavior of reinforcement and concrete. So, spatial average stress–strain relationship of concrete and reinforcement, and at the same time crack spacing, width and slip, can be computed through the proposed method.

The following conclusions can be summarized:

- The structural response and the spatial average behavior of reinforcement and concrete in RC elements reinforced with welded wire mesh strictly depend on the wire spacing and type of reinforcements. For welded wire mesh with wire spacing less than 20 times of wire diameter, the crack spacing is independent on the type of reinforcements and bond performance, and for larger wire spacing, the bond stress controls the cracking behavior of the elements.
- Generally, the tension stiffening of welded wire mesh with small wire spacing is higher than the RC elements reinforced with deformed bars, however, its value depends on the crack inclination.
- Welded wire mesh, shows smaller crack spacing and crack width compared to conventional reinforcing bars, however it has smaller structure ductility.
- The proposed method can be used for the design of welded wire modules to have an acceptable cracking response and structural ductility and also to construct macro models for nonlinear finite element analysis.

References

[1] Ayyub BM, Chang PC. Welded wire fabric for bridges. I. Ultimate strength and ductility. J Struct Engng 1994;120(6):1866–81.
[2] Lee SL, Mansur MA, Tan KH, Kasiraju K. Cracking behavior of concrete tension members reinforced with welded wire fabric. ACI Struct J 1987;84(6):481–91.
[3] Griezic A, Cook WD, Mitchell D. Tests to determine performance of deformed welded wire fabric stirrups. ACI Struct J 1994;91(2):211–20.
[4] Vecchio FJ, Collins MP. The response of reinforced concrete to in-plane shear and normal stresses. Publication no. 82-03, University of Toronto, 1982.
[5] Vecchio FJ, Collins MP. The modified compression field theory for reinforced concrete elements subjected to shear. ACI J 1986;83(2):219–31.
[6] Vecchio FJ, Chan CCL. Reinforced concrete membrane elements with perforations. J Struct Engng 1990;116(9):2344–60.
[7] Belleti B, Cerioni R. Physical approach for reinforced-concrete (PARC) membrane elements. J Struct Engng 2001;127(12):1412–26.
[8] Kaufmann W, Marti P. Structural concrete: cracked membrane model. J Struct Engng 1998;124(12):1467–75.
[9] Okamura H, Maekawa K. Nonlinear analysis and constitutive models of reinforced concrete. Tokyo, Japan: Gihodo-Shuppan; 1991.
[10] Shima H, Chou L, Okamura H. Micro and macro models for bond in reinforced concrete. J Faculty Engng, Univ Tokyo (B) 1987;39(2):133–94.
[11] Salem H. Enhanced tension stiffening model and application to nonlinear dynamic analysis of reinforced concrete. Doctoral dissertation, Department of Civil Engineering, The University of Tokyo, 1998.
[12] CEB-FIP model code for concrete structure. Paris: Comite Euro-International Du Beton, 1990.
[13] Robins PJ, Standish IG. The influence of lateral pressure upon anchorage bond. Mag Concrete Res 1984;36(129):195–202.
[14] Walker PR, Batayneh MK, Regan PE. Bond strength tests on deformed reinforcement in normal weight concrete. Mater Struct 1997;30:424–9.
[15] Goto Y. Cracks formed in concrete around deformed tension bars. ACI J 1971;68(4):244–51.
[16] Qureshi J, Maekawa K. Computational model for steel embedded in concrete under combined axial pullout and transverse shear displacement. Proc of JCI 1993;15(2):1249–54.
[17] Shin H. Finite element analysis of reinforced concrete members subjected to reversed cyclic in-plane loadings. Doctoral dissertation, Department of Civil Engineering, The University of Tokyo, 1988.
[18] Qureshi J. Modeling of stress transfer across reinforced concrete interfaces. Doctoral dissertation, Department of Civil Engineering, The University of Tokyo, 1993.
[19] Dei Poli S, Di Prisco M, Gambarova PG. Shear response, deformation and subgrade stiffness of a dowel bar embedded in concrete. ACI Struct J 1992;89(6):665–75.
[20] Soroushian P, Obaseki K, Rojas MC. Bearing strength and stiffness of concrete under reinforcing bars. ACI Mater J 1987;84(3):179–84.
[21] Fantilli AP, Ferretti D, Iori I, Vallini P. Behavior of R/C elements in bending and tension: the problem of minimum reinforcement ratio. In: Carpiniteri A, editor. Minimum reinforcement in concrete members, Vol. 24. Torino, Italy: ESIS Publication; 1991. p. 99–125.
[22] Ushida Y, Rokugo K, Koyanagi W. Determination of tension softening diagrams of concrete by means of bending tests. Proc JSCE 1991;14(426):203–12.
[23] Maekawa K, Okamura H. The deformational behavior and constitutive equation of concrete using the elasto-plastic and fracture model. J Faculty Engng, Univ Tokyo (B) 1983;37(2):253–328.
[24] Bujadham B, Maekawa K. The universal model for stress transfer across cracks in concrete. Proc JSCE 1992;17(451):277–87.
[25] Li B, Maekawa K, Okamura H. Contact density model for stress transfer across cracks in concrete. J Faculty Engng, Univ Tokyo (B) 1989;40(1):9–52.
[26] Rizkalla S, Hwang L. Crack prediction for members in uniaxial tension. ACI J 1984;88(44):572–9.
[27] Zararis PD. Concrete shear failure in reinforced concrete elements. J Struct Engng 1996;122(9):1006–15.
[28] American Concrete Institute. Building code requirements for structural concrete (ACI318-95) and commentary (ACI318R-95). Detroit, American Concrete Institute, 1995.